New neutrino physics and the altered shapes of solar neutrino spectra

Ilídio Lopes*

Centro Multidisciplinar de Astrofísica, Instituto Superior Técnico, Universidade de Lisboa, Avenue Rovisco Pais, 1049-001 Lisboa, Portugal

(Received 25 August 2016; published 26 January 2017)

Neutrinos coming from the Sun's core have been measured with high precision, and fundamental neutrino oscillation parameters have been determined with good accuracy. In this work, we estimate the impact that a new neutrino physics model, the so-called generalized Mikheyev-Smirnov-Wolfenstein (MSW) oscillation mechanism, has on the shape of some of leading solar neutrino spectra, some of which will be partially tested by the next generation of solar neutrino experiments. In these calculations, we use a high-precision standard solar model in good agreement with helioseismology data. We found that the neutrino spectra of the different solar nuclear reactions of the pp chains and carbon–nitrogen–oxygen cycle have quite distinct sensitivities to the new neutrino physics. The HeP and ^8B neutrino spectra are the ones in which their shapes are more affected when neutrinos interact with quarks in addition to electrons. The shapes of the ^{15}O and ^{17}F neutrino spectra are also modified, although in these cases the impact is much smaller. Finally, the impact in the shapes of the PP and ^{13}N neutrino spectra is practically negligible.

DOI: 10.1103/PhysRevD.95.015023

I. INTRODUCTION

Since their discovery in 1956, neutrinos have always surprised physicists due to their unexpected properties, often challenging our basic understanding of the standard model of particle physics (in the remainder of the article, it will be called simply the "standard model") and the properties of elementary particles. In particular, the discovery of neutrino flavor oscillations stands as one of the most convincing proofs that the standard model is incomplete as it does not explain all the known experimental properties of the fundamental particles.

The neutrino research success has been made possible mostly due to many dedicated experiments performed during the last 50 years. It is worth highlighting the contributions of some pioneering experiments, among others, such as the Super-Kamiokande detector [1,2] where the oscillation of atmospheric neutrinos was discovered, and the SNO detector [3] where the fluxes of all neutrino flavor species produced in the Sun's core were measured for the first time. Many other experiments done during the previous decades have contributed to the success of this story, in particular, the solar neutrino experiments. Despite their technical complexities, these experiments were able to measure the electron-neutrino fluxes coming from the Sun and played a major role in the establishment of the so-called solar neutrino problem—a discrepancy between the theoretical prediction of neutrino fluxes and their experimental measurements, the experimental value being one third of the predicted value. This fact was evidenced for the first time by the Homestake experiment of Davis *et al.* [4], and confirmed by many other experiments that followed. It was the solar neutrino problem that prompted the development of the neutrino flavor oscillation model.

If indeed the previous generation of solar neutrino detectors has been one of the beacons of particle physics, both by leading the way in uncovering the basic properties of particles, including the nature of neutrino flavor oscillations, and by being responsible for developing pioneering techniques in experimental neutrino detection [5], the next generation of detectors is equally promising in discovering new physics. Among various, some of which will be looking for evidence of neutrino new physics, we can mention the following future detectors: the Low Energy Neutrino Astronomy (LENA) [6], the Jiangmen Underground Neutrino Observatory (JUNO) [7], the Deep Underground Neutrino Experiment (DUNE) [8], the NOνA Neutrino Experiment [9], and the Jinping Neutrino Experiment [10].

These detectors will measure with high precision the neutrino fluxes and neutrino spectra of a few key neutrino nuclear reactions, such as the ^{8}B electron-neutrino (^{8}Bν_e) spectrum produced by the β-decay process in the ^{8}B solar (chain) reaction: $^7Be(p,\gamma)^8(e^+\nu_e)^8B^*(\alpha)^4He$ [11,12]. This will allow us to probe in detail the Sun's core, including the search for new neutrino physics interactions or even new physics processes. Moreover, the high quality of the data will enable the development of inversion techniques for determining basic properties of the solar plasma (e.g., [13]). Specific examples can be found in Balantekin *et al.* [14] and Lopes [15]. Equally, solar neutrino data can be used to find specific features associated with possible new physical processes present in the Sun's interior (e.g., [16]), such as the possibility of an isothermal solar core associated with the presence of dark matter [17].

Today, the basic principles of neutrino physics are firmly established: neutrinos are massive particles with

*ilidio.lopes@tecnico.ulisboa.pt

 © 2017 American Physical Society

a mix of lepton flavors. The parameters describing neutrino flavor oscillations have been measured with great accuracy and precision, which has been possible due to the extensive studies made by many different types of neutrino experiments: solar and atmospheric neutrino observatories, nuclear reactors and experimental particle accelerators (e.g., [18–20]). Section III C presents the status of the current neutrino oscillation parameters obtained from up-to-date experimental data.

Even if many properties of neutrinos are known, many others are still a mystery. Firstly, are neutrinos Majorana or Dirac fermions, i.e., are neutrinos their own antiparticle? Although the theoretical expectation favors the first option, only experimental evidence can settle this question. Secondly, what is the mass hierarchy of neutrinos? In other words, does the order of neutrino masses between the different particle families follow a normal hierarchy (two light neutrinos followed by a heavier one) or an inverted hierarchy (one light neutrino followed by two heavier ones)?

Together with the CP violation in the lepton sector, these are the most important questions of neutrino physics. Some of these questions will be answered by the next generation of neutrino experiments—the long baseline neutrino experiments and solar neutrino telescopes. Nevertheless, it is necessary to improve the current neutrino flavor model to take full advantage of the forthcoming experimental data.

Despite the success of the current neutrino physics model in explaining most of the neutrino's known observed properties, the solution encountered clearly indicates the existence of new physics beyond the standard model. As such, this implies that within the current particle physics theoretical framework, experiments can study neutrinos in other types of interactions. When such processes occur, these lead to important modifications of the physical mechanisms by which neutrinos are created, propagate and interact with other particles of the standard model. This new class of neutrino interactions is usually known as nonstandard interactions (NSI).

The nonstandard interactions of neutrinos have been extensively studied in the literature, among other reviews on this topic; see for instance the work of Miranda and Nunokawa [21] and Ohlsson [22]. Moreover, the constraints on the NSI parameters and their effects for low-energy neutrinos have been derived from a great variety of experimental results. Until now no definitive evidence of nonstandard interactions has been provided by the experimental data. Actually, all observations made as yet can be explained in terms of the standard interactions of the three known neutrinos, although some of them need the help of sterile neutrinos. Nevertheless, in some cases the nonstandard interactions of neutrinos provide an interesting and valid alternative (e.g., [23]).

In this work we are mostly concerned with the nonstandard interactions of solar neutrinos. These interactions can affect the neutrino production inside the Sun, the detection of neutrinos by experimental detectors and the neutrino propagation in the Earth's and Sun's interiors. In particular, our study focus on the propagation of neutrinos through baryonic matter in the Sun's interior, a process usually known as the generalized Mikheyev-Smirnov-Wolfenstein (MSW) oscillation mechanism, or generalized matter effect oscillations. Our goal is to make predictions about the modifications imprinted by this new generalized MSW on the shape of the solar neutrino spectrum produced by some of the pp and carbon–nitrogen–oxygen (CNO) key nuclear reactions, like HeP and ^8B neutrino spectra.

The high quality of the standard solar model in reproducing the measured solar neutrino fluxes, and the observed acoustic frequency oscillations, makes it a privileged tool to look for the new interactions within a generalized Mikheyev-Smirnov-Wolfenstein mechanism occurring in the Sun's interior. The standard solar model (SSM) [24], partly validated by helioseismology, predicts that the density inside the Sun varies from about 150 $\mathrm{g\,cm^{-3}}$ in the center of the star, to 1 $\mathrm{g\,cm^{-3}}$ at half of the solar radius. The variation of density of matter with the solar radius is followed by identical variations on the local quantities of electrons and quarks. Moreover, the different type of quarks will also be affected by the local distribution of chemical elements (most noticeably hydrogen and helium) which lead to a nonobvious distribution of up and down quarks. Therefore, we can anticipate that the current standard solar model, combined with data coming from the next generation of solar neutrino detections, will allow us to put much stronger constraints on the nonstandard interactions of neutrinos.

In the next section, we review the current status of the standard solar model and neutrino production in the Sun's core. In Sec. III, we present a summarized discussion about the current standard neutrino oscillation flavor model, and a generalized model for which neutrinos have new types of interactions with standard particles. In Sec. IV, we compute the neutrino spectra resulting from these new types of interactions. In the final section we discuss the results and their implications for future neutrino experiments.

II. NEUTRINO PRODUCTION IN THE SUN'S CORE

A. Helioseismology and the standard solar model

During the last three decades helioseismology has provided solar physics with a tool that describes with unprecedented quality the internal structure of the Sun from its surface down to the deepest layers of the Sun's interior. This has allowed astronomers to characterize with great precision the different solar neutrino sources. Equally, this discipline has stimulated the development of inversion techniques to probe the internal solar dynamics. Today an impressive agreement has been reached between the neutrino flux predictions and the neutrino flux measurements made by the existing neutrino detectors. The high quality of the helioseismology data has allowed researchers to compute an exceptionally accurate model of the Sun's interior—the standard solar model. The neutrino flux predictions of the solar model have an accuracy comparable to the current measurements made by particle accelerators or nuclear reactors.

The standard solar model in this study is obtained using a version of the one-dimensional stellar evolution code CESAM [25]. The code has an up-to-date and very refined microscopic physics (updated equation of state, opacities, nuclear reactions rates, and an accurate treatment of the microscopic diffusion of heavy elements), including the solar mixture of Asplund *et al.* [26,27]. This solar model is calibrated to reproduce with high accuracy the present total radius, luminosity and mass of the Sun at the present $t_\odot = 4.54 \pm 0.04$ Gyr [28]. Moreover, this model is required to have a fixed value of the photospheric ratio $(Z/X)_\odot$, where X and Z are the mass fraction of hydrogen and the mass fraction of elements heavier than helium. This solar standard model shows acoustic seismic diagnostics and solar neutrino fluxes similar to other models found in the literature [24,29–34].

This solar model is calibrated for the present day solar data with a high accuracy. Therefore slightly different physical assumptions will lead to different radial profiles of temperature, density and chemical composition, among other quantities. These changes result from readjustments of the Sun's internal structure caused by the need to obtain the same total luminosity. In particular, the neutrino fluxes and sound speed profile will be very sensitive to the radial distributions of the previous quantities. As such, using the high precision data from helioseismology, it is possible to put strong constraints to the internal structure of the Sun and its neutrino fluxes [28,35].

The current uncertainty between the square of the sound speed profile inferred from helioseismology acoustic data and the one obtained from the standard solar model using the up-to-date photospheric abundances Asplund *et al.* [27] is smaller than 3% for any layer of the Sun's interior. Although there is a difference between the sound speed profile computed using an older mixture of abundances by Grevesse and Sauval [36] or the new mixture of Asplund *et al.* [27], for this study these effects are negligible on the radial variation of electrons, protons and neutrons. This has become even more so, since recent measurements of the solar metallicity abundances suggest that the sound speed difference between helioseismic data and the standard solar model can be reduced further [37].

Particularly relevant for our study is the radial profile of the electron, proton and neutron densities inside the Sun, since these quantities are fundamental ingredients to test the nonstandard neutrino physics theories.

B. The solar neutrino sources

The neutrino fluxes produced in the nuclear reactions of the pp chains and CNO cycle have been computed for an updated version of the solar standard model, as discussed in the previous section. Figure 1 shows the location of the different neutrino emission regions of the nuclear reactions for an up-to-date SSM. In the Sun's core, the neutrino emission regions occur in a sequence of shells, following closely the location of nuclear reactions, orderly arranged in a sequence dependent on their temperature. The helioseismology data and solar neutrino fluxes guarantee that such neutrino shells are known with a great accuracy. The leading source of the energy in the present Sun is the pp chain nuclear reactions, since the CNO cycle nuclear reactions contribute with less than 2%. The first reaction of the pp chains is the PP-ν reaction which has the largest neutrino emission shell, a region that extends from the center to $0.30R_\odot$. The PeP-ν reaction has a neutrino emission shell which is similar to the PP reaction, but with a shell of $0.25R_\odot$. These nuclear reactions are strongly dependent on the total luminosity of the star. Alternatively, the neutrino emission shells of ${}^8B$-ν and ${}^7Be$-ν extend up to $0.15R_\odot$ and $0.22R_\odot$. It is interesting to notice that the maximum emission of neutrinos for the pp chain nuclear reactions follows an ordered sequence (see Fig. 1): ${}^8B$-ν, ${}^7Be$-ν, PeP-ν and PP-ν with the maximum emissions located at 0.05, 0.06, 0.08 and $0.10R_\odot$. The known neutrino emission shells of the different CNO cycle nuclear reactions are the following: ${}^{15}O$-ν, ${}^{17}F$-ν and ${}^{13}N$-ν. These shells are similar to the ${}^8B$-ν emission shell. The ${}^{13}N$-ν have

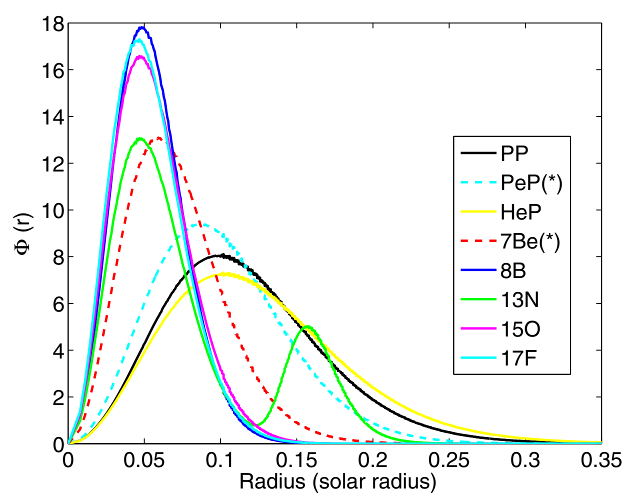

FIG. 1. The electron-neutrino fluxes produced in the various nuclear reactions of the pp chains and CNO cycle. These neutrino fluxes were calculated for a standard solar model using the most updated microscopic physics data. This solar model is in agreement with the most current helioseismology diagnostic and other solar standard models published in the literature (see text). For each neutrino type j [with $j = PP, PeP(*), HeP, {}^8B, {}^7Be(*), {}^{13}N, {}^{15}O, {}^{17}F$], $\Phi_j(r) \equiv (1/F_j) df_j(r)/dr$ is drawn as a function of the fractional radius r for which f_j is the flux in s^{-1} and F_j is the total flux for this neutrino type. The neutrino sources noted with the symbol $(*)$ correspond to spectral lines. The same color scheme is used in Figs. 4 and 5.

two independent shells: one in the Sun's deepest layers of the core and a second shell located between 0.12 and 0.25 of $R_\odot$. The emission of neutrinos for ^{15}O-ν, ^{17}F-ν and ^{13}N-ν shells is maximal at 0.04–0.05 of $R_\odot$. The ^{13}N-ν neutrinos have a second emission maximum which is located at $0.16R_\odot$.

C. Neutrinos, electrons and quarks

The electron density $n_e(r) = N_o\rho(r)/\mu_e(r)$ where μ_e is the mean molecular weight per electron, $\rho(r)$ the density of matter and N_o Avogadro's number. In this model we will consider the impact on the up and down quarks. Accordingly, the density of up and down quarks will be computed from a relation analogous to $n_e(r)$, $n_i(r) = N_o\rho(r)/\mu_i(r)$ (with $i = u$, d) where $\mu_i(r)$ is the mean molecular weight per quark given by

$$\mu_i(r) = \left[(1+\delta_{iu})X(r) + \frac{3}{2}Y(r) + \frac{3}{2}Z(r)\right]^{-1} \quad (1)$$

where $i = u$, d with $X + Y + Z = 1$. The distribution of electrons and up and down quarks, as a function of the radius of the Sun for the standard solar model, is shown in Fig. 2. The mean molecular weight per quark is dominated by hydrogen and helium since the only other elements included in Z like carbon, nitrogen, oxygen and heavier elements contribute with a very small fraction to the solar plasma. Although the Z variation can affect the evolution of the star in the way it affects the radiative transport [37], its impact on the standard and nonstandard MSW interactions for $\mu_i(r)$, $i = u, d$, is small since the relative radial variation between up and down quarks due to Z variation is not significant.

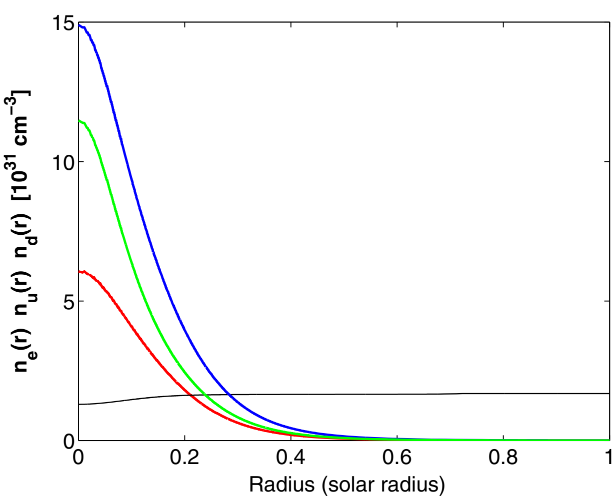

FIG. 2. The solar plasma is constituted mostly by electrons, protons and neutrons. The plot shows variation of the number density of electrons $n_e(r)$ (red curve), up quarks $n_u(r)$ (blue curve) and down quarks $n_d(r)$ (green curve), and the relative variation of up and down quarks $n_u(r)/n_d(r)$ (black curve). In the center $n_u/n_d = 1.3$ and near the surface $n_u/n_d = 1.7$.

III. MODEL OF NEUTRINO PHYSICS OSCILLATIONS

A. Basic neutrino physics

In the standard model, neutrinos interact with other particles only via weak standard interactions (SI), which are described by the Lagrangian $\mathcal{L}_{si}$ which can be decomposed into components describing the charged and neutral interactions [38–40]. Nevertheless, in the current study, we choose to write the Lagrangian $\mathcal{L}_{si}$ as an effective interaction Lagrangian [40,41], which at low and intermediate neutrino energies reads

$$\mathcal{L}_{si} = -2\sqrt{2}G_F g_P^f(\bar{\nu}_\alpha\gamma_\rho L\nu_\alpha)(\bar{f}\gamma^\rho P f) \quad (2)$$

where f denotes a lepton or a quark, such as the u quark and the d quark; ν_α are the three light neutrinos (where the subscript $\alpha = e, \mu, \tau$); P is the chiral projector [equal to R or L such that $R, L \equiv (1 \pm \gamma^5)/2$]; and g_P^f denotes the strength of the standard interaction (ns) as defined in the standard model, between neutrinos of flavors α and β and the P-handed component of the fermion f. Specifically, the g_P^f coupling (left- and right-handed coupling, i.e., g_L^f and g_R^f) for the u quark (and c and t quarks) to the Z boson corresponds to $g_L^u = 1/2 - 2/3\sin^2\theta_w$ and $g_R^u = -2/3\sin^2\theta_w$. Similarly, the g_P^f for the d quark (and s and b quarks) corresponds to $g_L^d = -1/2 + 1/3\sin^2\theta_w$ and $g_R^d = 1/3\sin^2\theta_w$; the g_P^f for the electron corresponds to $g_L^d = -1/2 + \sin^2\theta_w$ and $g_R^d = \sin^2\theta_w$; and the g_P^f for the neutrino (ν_α with $\alpha = e, \mu, \tau$) corresponds to $g_L^d = 1/2$ and $g_R^d = 0$. θ_w is the Weinberg mixing angle [42,43], with a typical value of $\sin^2\theta_w \approx 0.23$ [44].

The evolution of a generic neutrino state $\nu_\alpha \equiv (\nu_e\nu_\mu\nu_\tau)^T$ is described by a Schrödinger-like equation [38] that expresses the evolution of the neutrino between the flavor states [38] with the distance r, from neutrinos that are produced in the Sun's core until their arrival at the Earth's neutrino detectors. The equation reads

$$i\frac{d\nu_\alpha}{dr} = \mathcal{H}\nu_\alpha = (\mathcal{H}_v + \mathcal{H}_m)\nu_\alpha, \quad (3)$$

where $\mathcal{H}$ is the total Hamiltonian; $\mathcal{H}_v$ and $\mathcal{H}_m$ are the Hamiltonian component expressions for vacuum and in matter flavor variations, such that $\mathcal{H}_v \equiv M_\nu^\dagger M_\nu/2p_\nu$ where M_ν is the mass matrix of neutrinos (the term proportional to the neutrino momentum p_ν is omitted here); and $\mathcal{H}_m$ is the Hamiltonian (a diagonal matrix of effective potentials) which depends on the properties of the solar plasma, i.e., the density and composition of the matter, such that $\mathcal{H}_m = \mathrm{diag}(V_e, V_\mu, V_\tau)$.

The flavor evolution is described in terms of the instantaneous eigenstates of the Hamiltonian in matter $\nu_m \equiv (\nu_{1m}, \nu_{2m}, \nu_{3m})^T$. These eigenstates are related to the flavor states by the mixing matrix in matter, U_m: $\nu_\alpha = U^m\nu_m$.

B. The effective matter potential

As neutrinos propagate in the Sun's interior, they will oscillate between the three flavor states ν_e, ν_μ and ν_τ due to vacuum oscillations; however in the highly dense medium which is the Sun's interior, contrary to their propagation in vacuum, the scattering of neutrinos with other elementary particles, like electrons, will enhance their oscillation between flavor states. Indeed, neutrinos propagating in a dense medium like the Sun (or Earth) have their flavor between states affected by the coherent forward scattering, i.e., coherent interactions of the neutrinos with the medium background [38]. The interaction of neutrinos with the medium proceeds through coherent forward elastic charged-current (CC) and neutral-current (NC) scatterings, which as usual are represented by the effective potentials V_α^{cc} and V_α^{nc} for each of the three types of neutrinos.

Therefore, at low energies, the potentials can be evaluated by taking the average of the effective four-fermion Hamiltonian due to the exchange of W and Z bosons over the state describing the background medium. Accordingly, for a nonrelativistic unpolarized medium, for the effective potential of ν_e, ν_μ and ν_τ neutrinos, one obtains

$$V_\alpha = V_\alpha^{cc} + V_\alpha^{nc}, \tag{4}$$

where $\alpha = e, \mu, \tau$.

Let us consider that the solar internal medium is mainly composed of electrons, up quarks and down quarks as in protons and neutrons with the corresponding $n_e(r)$, $n_u(r)$ and $n_d(r)$ local number densities. The contribution to $\mathcal{H}_m$ due to the cc scattering of electron neutrinos ν_e (produced in the Sun's core) propagating in a homogeneous and isotropic gas of unpolarized electrons (like the electron plasma found in the Sun's interior) is given by

$$V_e^{cc} = \sqrt{2} G_F n_e(r) \tag{5}$$

where G_f is the Fermi constant. For ν_μ and ν_τ, the potential due to its cc interactions is zero for most of the solar interior since neither μ's nor τ's are present; therefore,

$$V_\mu^{cc} = V_\tau^{cc} = 0. \tag{6}$$

Generically, for any active neutrino, the V_α^{cc} reads

$$V_\alpha^{cc} = \delta_{\alpha e} \sqrt{2} G_F n_e(r). \tag{7}$$

Analogously, one determines V_α^{nc} for any neutrino due to NC interactions. Since NC interactions are flavor independent, these contributions are the same for neutrinos of all three flavors. The neutral-current potential reads

$$V_\alpha^{nc} = \sum_f \sqrt{2}\, G_F g_v^f n_f(r) \tag{8}$$

where $\alpha = e, \mu, \tau$ and $f = e, u, d$. $n_f(r)$ is the number density of fermions, electrons, up quarks (u) and down quarks (d) as in protons (uud) and neutrons (udd). The factors g_v^f are the axial coupling to fermions ($g_v^e = -1/2 + 2\sin^2\theta_w$, $g_v^u = 1/2 - 4/3 \sin^2\theta_w$ and $g_v^d = -1/2 + 2/3 \sin^2\theta_w$; see for example Giunti and Chung [45]). Therefore the effective potential [38] for any active neutrino due to the neutral-current V_α^{nc} reads

$$V_\alpha^{nc} = \sqrt{2} G_F [g_v^e n_e(r) + g_v^u n_u(r) + g_v^d n_d(r)], \tag{9}$$

where $n_u(r)$ and $n_d(r)$ are the analogues of $n_e(r)$, i.e., the number density of up quarks and down quarks in the Sun's interior.

Using Eqs. (7) and (8) in Eq. (4), the effective potential for any active neutrino crossing the solar plasma reads

$$V_\alpha = \sqrt{2} G_F [\delta_{\alpha e} n_e + g_v^e n_e + g_v^u n_u + g_v^d n_d]. \tag{10}$$

When neutrinos propagate through matter, the forward scattering of neutrinos off the background matter will induce an index of refraction for neutrinos. This is the exact analogue to the index of refraction of light traveling through matter. However, the neutrino index of refraction will depend on the neutrino flavor, as the background matter contains different amounts of scatters for the different neutrino flavors.

The effective potentials V_α are due to the coherent interactions of active flavor neutrinos with the medium through coherent forward elastic weak CC and NC scatterings.

Inside the Sun, as local matter is composed of neutrons, protons, and electrons, the effective potential V_α for the different neutrino species (including ν_e neutrinos) has a quite distinct form which depends on the local number densities $n_e(r)$, $n_u(r)$ and $n_d(r)$, quantities which depend on the chemical composition (its metallicity Z) of the Sun's interior. Nevertheless, at first approximation, since electrical neutrality implies locally an equal number density of protons (uud) and electrons, V_α takes a more simple form [Eq. (10)], as the NC potential contributions of protons and electrons cancel each other. Therefore, only neutrons (udd) contribute to V_α^{nc}. Hence the last two terms of Eq. (9) can be expressed as $g_v^n n_n(r)$ to only take into account the quark contribution for neutrons. In this expression $n_n(r)$ is the local density of neutrons and g_v^n is the neutron coupling constant, it follows that $g_v^n = g_v^u + 2g_v^d = -1/2$, and Eq. (9) reads $V_\alpha^{nc} = -\sqrt{2}/2 G_F n_n(r)$. Now V_α [Eq. (10)] inside the Sun yields

$$V_\alpha = \sqrt{2} G_F \left[\delta_{\alpha e} n_e(r) - \frac{1}{2} n_n(r)\right], \tag{11}$$

where $\alpha = e, \mu, \tau$.

As we will discuss later, only effective potential differences affect the propagation of neutrinos in matter [46]; accordingly, one defines the potential difference between two neutrino flavors α and β as

$$V_{\alpha\beta} = V_\alpha - V_\beta, \quad (12)$$

where $\alpha, \beta = e, \mu, \tau$.

The Sun's interior is a normal medium composed of nuclei (protons and neutrons) and electrons. Since the effective potential for muon and tau neutrinos, V_α (with $\alpha = \mu, \tau$ or a combination thereof) is due to the neutral current scattering only [see Eq. (11)], this leads to $V_{\mu\tau} = V_\mu - V_\tau = 0$. However, as the effective potential for electron neutrinos depends on the neutral and charged current scatterings, in this case

$$V_{e\alpha} = \sqrt{2} G_F n_e(r), \quad (13)$$

where $\alpha = \mu, \tau$ or a combination thereof. Although for the Sun and Earth charged current interactions with electrons are the only effective potential that contributes to the propagation of electron neutrinos, there are other types of nontypical matter, like the one found in the core of supernovae and in the early Universe for which the effective potential difference $V_{\alpha\beta}$ has a much stronger dependence on the properties of the background plasma [43,46].

C. Neutrino oscillation data parameters

As shown in the previous section, the neutrino flavor oscillation model is described with the help of six mixing parameters, all of which have been determined from experimental data [47]. The quantities are the following: the difference of the squared neutrino masses Δm^2_{21}, Δm^2_{31}; the mixing angles $\sin^2\theta_{12}, \sin^2\theta_{13}, \sin^2\theta_{23}$; and the CP-violation phase δ_{CP}.

The mass square differences and mixing angles are known with a good accuracy [48,49]: Δm^2_{31} is obtained from the experiments of atmospheric neutrinos and Δm^2_{12} is obtained from solar neutrino experiments.

The mixing angles are not uniformly well defined: θ_{12} was obtained from solar neutrino experiments with an excellent precision; θ_{23} was obtained from atmospheric neutrino experiments (this is the mixing angle with the highest value); θ_{13} was first estimated in the Chooz reactor [50], but its value is very small and is still very uncertain [51]. Nowadays with Daya Bay and Reno, the situation has largely improved [52]. However, present experiments cannot fix the value of the CP-violation phase [53].

An overall fit to the data obtained from the different neutrino experiments (solar neutrino detectors, accelerators, atmospheric neutrino detectors and nuclear reactor experiments) suggests that the parameters of neutrino oscillations are the following [48,49]: $\Delta m^2_{31} \sim 2.457 \pm 0.04510^{-3}\ eV^2$ or ($\Delta m^2_{31} \sim -2.449 \pm 0.04810^{-3}\ eV^2$), $\Delta m^2_{21} \sim 7.500 \pm 0.01910^{-5}\ eV^2$, $\sin^2\theta_{12} = 0.304 \pm 0.013$, $\sin^2\theta_{13} = 0.0218 \pm 0.001$, $\sin^2\theta_{23} = 0.562 \pm 0.032$ and $\delta_{CP} = 2\pi/25n$ with $n = 1, \ldots, 25$.

In the limiting case where the value of the mass differences, Δm^2_{12} or Δm^2_{31}, is large, or one of the angles of mixing (θ_{12}, θ_{23}, θ_{31}) is small, the theory of three neutrino flavor oscillations reverts to an effective theory of two neutrino flavor oscillations [53]. Balantekin and Yuksel have shown that the survival probabilities of solar neutrinos calculated in a model with two neutrino flavor oscillations or with three neutrino flavor oscillations have very close values [54].

D. The survival of electron neutrinos

Mostly motivated by solar neutrino data, the focus of this work is the study of the propagation of electron neutrinos, in particular to determine the survival probability of electron neutrinos P_e [$\equiv P(\nu_e \to \nu_e)$] arriving to Earth which have their flavor changed due to vacuum and solar matter oscillations. Luckily, in the Sun P_e takes a particularly simple form, since the evolution of neutrinos in matter is adiabatic and for that reason their contribution for P_e can be cast in a similar manner to the vacuum-oscillation expression. Accordingly, the standard parametrization of the neutrino mixing matrix leads to the following survival probabilities for electron neutrinos: P_e reads

$$P_e = c^2_{13} c^{m2}_{13} P^{ad}_2 + s^2_{13} s^{m2}_{13} \quad (14)$$

where $c_{ij} = \cos\theta_{ij}$, $s_{ij} = \sin\theta_{ij}$, and P^{ad}_2 reads

$$P^{ad}_2 = \frac{1}{2}(1 + \cos(2\theta_{12})\cos(2\theta^m_{12})). \quad (15)$$

The matter angles, θ^m_{12} and θ^m_{13}, which depend equally of the fundamental parameters of neutrino flavor oscillation and the properties of solar plasma are determined as follows:

(i) The mixing angle θ^m_{12} is determined by

$$\cos(2\theta^m_{12}) = -\frac{V^\star_{12}}{\sqrt{V^{\star 2}_{12} + (A^{\star -1}_{12}\sin(2\theta_{12}))^2}} \quad (16)$$

where the effective potential $V^\star_{12}(E, r)$ reads

$$V^\star_{12}(E, r) = c^2_{13} - A^{\star -1}_{12}\cos(2\theta_{12}) \quad (17)$$

where $A^\star_{12} = A_\star/\Delta m^2_{12}$ and $A_\star = 2EV_{\alpha\beta}$ [38]. The parameter $A_\star(E, r)$ contains the effect of matter on the electron-neutrino propagation as defined by $V_{\alpha\beta}$, given by Eq. (13). In the specific case of electron neutrinos, $A_\star(E, r) = 2E\sqrt{2}G_F n_e(r)$ [with $V_{e\alpha} = \sqrt{2}G_F n_e(r)$].

(ii) The mixing angle θ^m_{13}, according to Goswami and Smirnov [55], is determined by

$$\sin^2(\theta^m_{13}) \approx \sin^2(\theta_{13})[1 + 2A^\star_{13}] \quad (18)$$

with $A^\star_{13} = 2EV^o_e/\Delta m^2_{31}$, where V^o_e is the effective potential at the electron-neutrino production radius

r_o, i.e., $V_e^o = \sqrt{2}G_F n_e(r_o)$. The value of r_o is different for the different neutrino sources of the pp chains and CNO cycle.

E. New neutrino physics

In the presence of physics beyond the standard model (e.g., [56]), the neutral current interactions that are flavor diagonal and universal in the standard model can have a more general form. Hence, new interactions arise between neutrinos and matter, which conveniently one defines as NSI; these new neutrino interactions with fermions are described by a new effective Lagrangian (e.g., [41,57,58]). Accordingly, the classical Lagrangian [Eq. (2)] is generalized to take into account these new types of interactions previously forbidden. The new Lagrangian reads

$$\mathcal{L}_{nsi} = -2\sqrt{2}G_F \epsilon_{\alpha\beta}^{fP}(\bar{\nu}_\alpha \gamma_\rho L \nu_\beta)(\bar{f}\gamma^\rho P f) \tag{19}$$

where $\epsilon_{\alpha\beta}^{fP}$ is the equivalent of g_P^f for the standard interactions [Eq. (2)], which corresponds to the parametrization of the strength of the nonstandard interactions between neutrinos of flavors α and β and the P-handed component of the fermion f (e.g., [56]). Without loss of generality we consider only neutrino interactions with up and down quarks (e.g., [59]). In the latter Lagrangian, $\epsilon_{\alpha\beta}^{fP}$ corresponds to two classes of nonstandard terms: flavor preserving nonstandard terms proportional to $\epsilon_{\alpha\alpha}^{fP}$ (known as nonuniversal interactions) and flavor changing terms proportional to $\epsilon_{\alpha\alpha}^{fP}$ with $\alpha \neq \beta$.

Since the atoms and ions of the solar medium in which neutrinos propagate are nonrelativistic, the vector part of the NSI operator gives the dominant contribution for the interactions of the neutrinos with the plasma of the Sun's interior, in which case the effective NSI coupling can be described by the following combination [57]: $\epsilon_{\alpha\beta}^f = \epsilon_{\alpha\beta}^{fL} + \epsilon_{\alpha\beta}^{fR}$. These new kinds of neutrino interactions lead to a new effective potential difference to describe the propagation of neutrinos in matter [59]. Accordingly, the effective potential difference $V_{\alpha\beta}$ is written as a generalization of the $V_{\alpha\beta}$ obtained in the standard case: Eqs. (11) and (13). Hence, $V_{\alpha\beta}$ reads

$$V_{\alpha\beta} = V_e \delta_{\alpha e}\delta_{\beta e} + \sqrt{2}G_F \sum_f \epsilon_{\alpha\beta}^f n_f(r) \tag{20}$$

where $\epsilon_{\alpha\beta}^f$ is the strength of NSI of neutrinos with the medium. A more detailed discussion about the relations between $\epsilon_{\alpha\beta}^f$ and $\epsilon_{\alpha\beta}^{fP}$ can be found in the work of Gonzalez-Garcia and Maltoni [57]. Usually, $\epsilon_{\alpha\beta}^f$ is considered as a free parameter to be adjusted to fit the solar observational data.

In this work, we study only the NSI of electron neutrinos (ν_e) with the solar plasma. Accordingly, as is common practice, we chose to take into account only the NSI coupling of electron neutrinos with the up quarks and down quarks of the solar plasma. Among others, Friedland *et al.* [60] have shown that the coupling of electron neutrinos with up quarks is parametrized by a set of two independent parameters $(\epsilon_N^u, \epsilon_D^u)$, and similarly the coupling of electron neutrinos with down quarks is parametrized by another set of two independent parameters $(\epsilon_N^d, \epsilon_D^d)$. Each of these parameters corresponds to a linear combination of the original parameters $\epsilon_{\alpha\beta}^f$ which defines the strength of the nonstandard neutrino interactions with fermions as defined in Eq. (19). In the Appendix we show the relation of ϵ_D^f and ϵ_N^f with the parameters $\epsilon_{\alpha\beta}^f$, for which f is either d or u since in our study we are only concerned about the interaction with down and up quarks of the solar plasma. A detailed account of the relevance of these quantities can be found in the works of Gonzalez-Garcia and Maltoni (e.g., [57]); Maltoni and Smirnov (e.g., [59]); and Friedland *et al.* (e.g., [60]).

As in the case of standard neutrino interactions, for these NSI the oscillations of neutrino flavor are still adiabatic, so the probability of electron-neutrino survival is given by Eq. (14). However, in this case the quantity $\cos(2\theta_m)$ has been redefined to take into account the new effective matter potential [59]; accordingly

$$\cos(2\theta_{12}^m) \approx -\frac{V_{nsi}^\star}{\sqrt{V_{nsi}^{\star 2} + (2r_f\epsilon_N^f + A_{12}^{\star -1}\sin(2\theta_{12}))^2}} \tag{21}$$

where $V_{nsi}^\star$ reads

$$V_{nsi}^\star(E,r) = c_{13}^2 - A_{12}^{\star -1}\cos(2\theta_{12}) - 2r_f\epsilon_D^f. \tag{22}$$

where $r_f(r) = n_f(r)/n_e(r)$. Figure 3 shows the variation of the ratios $r_u(r)$ and $r_d(r)$ inside the star. $r_d(r)$ is smaller

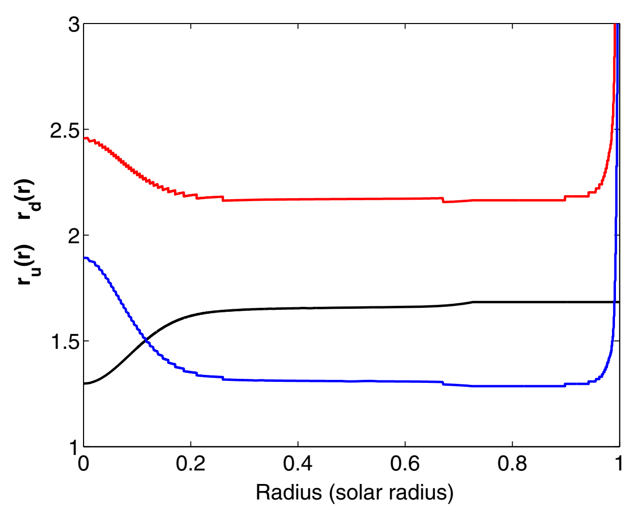

FIG. 3. Variation with the solar radius of the ratios $r_u(r) = n_u(r)/n_e(r)$ (red curve) and $r_d(r) = n_d(r)/n_e(r)$ (blue curve), and relative variation of up and down quarks $n_u(r)/n_d(r)$ (black curve).

than $r_u(r)$ because the star's composition is dominated by free protons (ionized hydrogen). As such, for each down quark there are two up quarks.

F. The electron-neutrino probability of survival

The neutrino emission reactions of the pp chains and the CNO cycle are produced at high temperatures in distinct layers in the Sun's core. Similarly, the neutrino flavor oscillations occur in the same regions. The average survival probability of electron neutrinos in each nuclear reaction region is given by

$$\langle P_e(E)\rangle_j = N_j^{-1}\int_0^{R_\odot} P_e(E,r)\phi_j(r)4\pi\rho(r)r^2 dr \tag{23}$$

where N_j is a normalization constant given by $N_j = \int_0^{R_\odot}\phi_j(r)4\pi\rho(r)r^2 dr$ and $\phi_j(r)$ is the electron-neutrino emission function for the j nuclear reaction. j corresponds to the following electron-neutrino nuclear reactions: PP, PeP, ^8B, ^7Be, ^{13}N, ^{15}O and ^{17}F. $\phi_j(r)$ defines the location where neutrinos are produced in each nuclear reaction j for which the production is maximum in the layer of radius r_j (cf. Fig. 1). The neutrino fluxes produced by the different nuclear reactions are sensitive to the local values of the temperature, molecular weight, density and electronic density. In this study, we consider that all neutrinos produced in the solar nuclear reactions are of electron flavor as predicted by standard nuclear physics; therefore, the local density of quarks only affects the $\langle P_e(E)\rangle_j$ by modifying the flavor of electron neutrinos by a new NSI like the generalized MSW mechanism.

The survival probability of electron neutrinos $\langle P_e(E)\rangle_j$ given by Eq. (23) is computed using Eqs. (14), (21) and (22). Figures 4 and 5 show $\langle P_e(E)\rangle_j$ for the different solar neutrino sources, either in the standard MSW or a generalized MSW. The different neutrino interaction models are described by a specific set of parameters: $(\epsilon_N^u, \epsilon_D^u, \epsilon_N^d, \epsilon_D^d)$. The top panels in Figs. 4 and 5 show $\langle P_e(E)\rangle_j$ for the standard MSW mechanism in which case all the parameters mentioned above are equal to zero. The other panels of Figs. 4 and 5 correspond to a generalized MSW mechanism for which the parameters $(\epsilon_N^u, \epsilon_D^u, \epsilon_N^d, \epsilon_D^d)$ can have values different from zero. Maltoni and Smirnov [59] among others have shown that only a relatively small ensemble of parameter combinations $(\epsilon_N^u, \epsilon_D^u, \epsilon_N^d, \epsilon_D^d)$ can be accommodated with the current set of neutrino flux observations. In this study, for convenience, we choose to focus on neutrino interactions for which electron neutrinos couple either with up quarks (for which $\epsilon_N^d = \epsilon_D^d = 0$) or with down quarks (for which $\epsilon_N^u = \epsilon_D^u = 0$). Specifically, we chose two fiducial sets of values ($\epsilon_N^f, \epsilon_D^f$, $f = u$, d) of the ensemble of parameters that fit simultaneously the solar and KamLAND neutrino data sets with good accuracy.

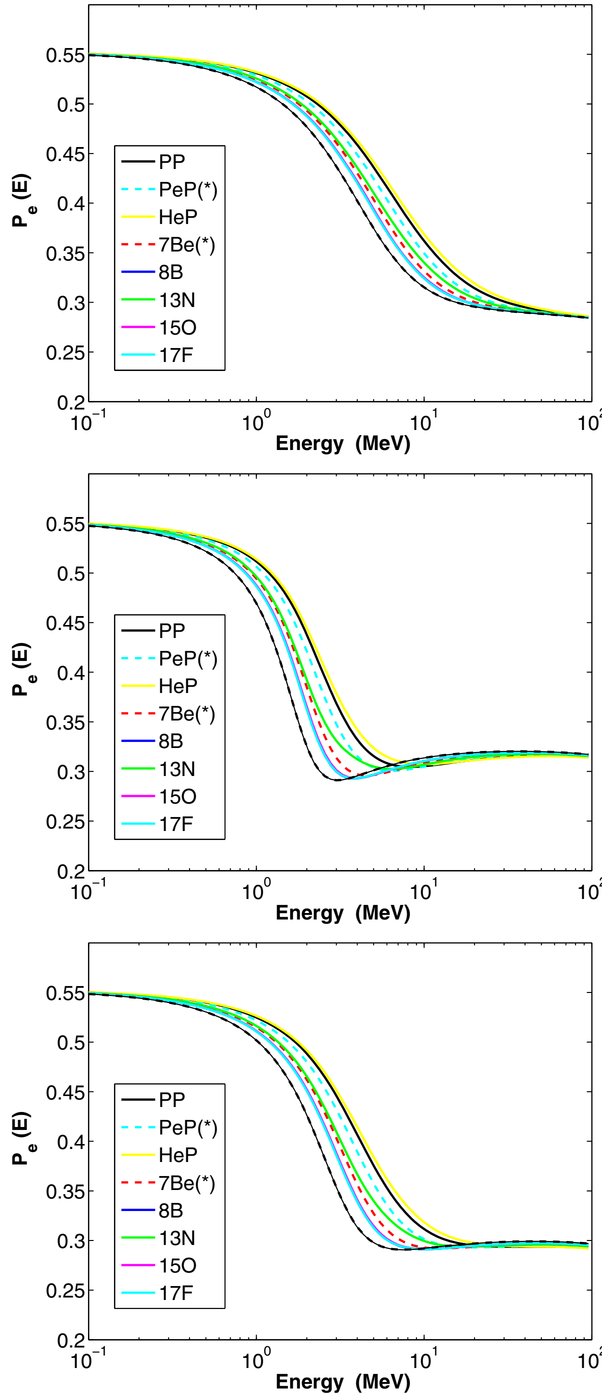

FIG. 4. The survival probability of electron neutrinos. The P_e curves correspond to neutrinos produced in the nuclear reactions located at different solar radii. The three panels correspond to the following neutrino models of interaction: SI with electrons (top panel); NSI with up quarks with the coupling constants, $\epsilon_N^u = -0.30$ and $\epsilon_D^u = -0.22$ (middle panel); and NSI with down quarks with coupling constant, $\epsilon_N^d = -0.16$ and $\epsilon_D^d = -0.12$ (bottom panel). The reference dotted black curve defines the survival probability of electron neutrinos in the center of the Sun for which the SI or NSI MSW flavor oscillation mechanism is maximum. The other colored curves follow the same color scheme shown in Fig. 1.

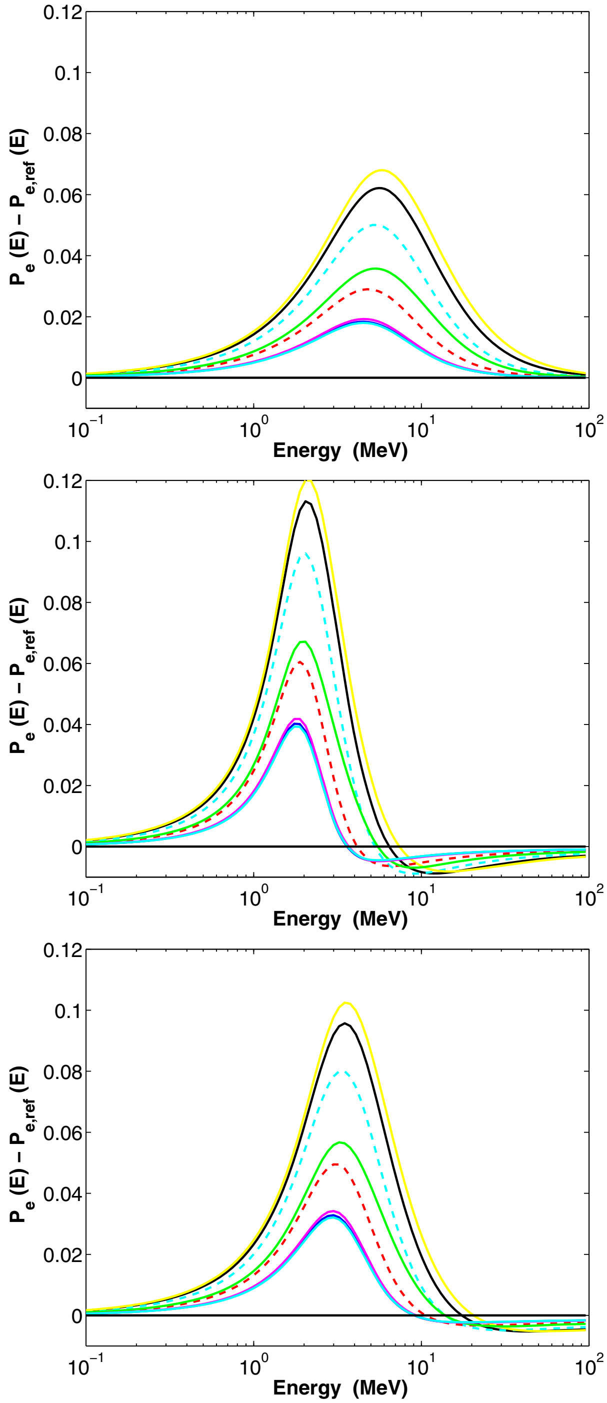

FIG. 5. The survival probability of electron neutrinos in a function of the neutrino energy for the different regions of emission. The different panels show the difference between the survival probability of the different electron-neutrino sources and the reference curve (dotted black curve in Fig. 4). The colored curves follow the same color scheme shown in Figs. 1 and 4.

Figure 4 shows the survival probability of electron neutrinos in the case of the NSI for the parameters sets ($\epsilon_N^u = -0.30, \epsilon_D^u = -0.22$) and ($\epsilon_N^d = -0.16, \epsilon_D^d = -0.12$). As discussed by Maltoni and Smirnov [59] these values correspond to the two parameters that best fit simultaneously the current solar and KamLAND neutrino data sets. The middle panels in Figs. 4 and 5 show $\langle P_e(E)\rangle_j$ for a neutrino up-quark interaction model, and the bottom panels in Figs. 4 and 5 show $\langle P_e(E)\rangle_j$ for a neutrino down-quark interaction model.

All the different neutrino interaction models have several common features. In general the $\langle P_e(E)\rangle_j$ are very similar for low- and high-energy neutrinos. It is only for neutrinos with intermediate energy that it is possible to distinguish between the different models (cf. Fig. 4). For neutrinos in this energy interval it is possible to distinguish between two effects: one is related to the location of the different neutrino sources, and a second effect is related to the parameter values ($\epsilon_N^u, \epsilon_D^u, \epsilon_N^d, \epsilon_D^d$) of the neutrino interaction model. In the former effect, the $\langle P_e(E)\rangle_j$ differentiation results from the fact that $\phi_j(r)$ are located at different solar radii, as shown in Fig. 1. Such an effect arises equally in SI and NSI neutrino interaction models. The second effect occurs only for NSI neutrino interaction models, and it is related to the radial distribution of up and down quarks (cf. Fig. 2).

This latter effect is shown in Figs. 4 and 5 for the two fiducial models adopted in this study: a pure neutrino up-quark model ($\epsilon_N^d = \epsilon_D^d = 0$) and a pure neutrino down-quark model ($\epsilon_N^u = \epsilon_D^u = 0$). Accordingly, for neutrinos with an intermediate energy, the $\langle P_e(E)\rangle_j$ corresponding to the neutrino up-quark interaction model has an impact of larger amplitude than the neutrino down-quark interaction model (compare the middle and bottom panels in Fig. 5). For instance, this effect is very significant for $\langle P_e(E)\rangle_{pp}$. Nevertheless, these preliminary results should be interpreted with caution, since each neutrino source only produces neutrinos within a limited range of energy; as such the NSI effect of $\langle P_e(E)\rangle_j$ shown in Fig. 5 can be significantly reduced in the final neutrino spectrum of some solar neutrino sources. Indeed, we recall that the neutrinos emitted by $\phi_j(r)$ are limited to a specific energy range for each j-nuclear reaction. As such only an energy portion of $\langle P_e(E)\rangle_j$ affects the final emitted neutrino spectrum. This point will be discussed in more detail in the next section.

IV. THE SOLAR ELECTRON-NEUTRINO SPECTRA

The solar energy spectrum of electron neutrinos from any specific nuclear reaction is known to be essentially independent of solar parameters; that is, the energy spectrum created by a specific nuclear reaction is the same independently of whether neutrinos are produced in an Earth laboratory or in the core of the Sun. Therefore, the neutrino energy spectrum of the different nuclear reactions can be assumed to be equivalent to its Earth laboratory counterpart. A typical example of such spectra is the ^{8}B neutrino energy spectrum emitted by the ^{8}B nuclear reaction of the pp chains in the Sun's core. This solar neutrino spectrum has been shown to be equivalent to several experimental determinations of the ^{8}B neutrino spectrum (e.g., [61,62]). Bahcall and Holstein [63], Napolitano *et al.* [64], among others, have shown that the ^{8}B neutrino spectrum emitted in the Sun's core is equal to the spectrum measured in the laboratory, as the surrounding solar plasma does not affect this type of nuclear reaction. The ^{8}B neutrino spectrum measured in the laboratory agrees remarkably well with its theoretical prediction for neutrinos with an energy below 12 MeV, a small difference appearing only for high-energy neutrinos. The experimental ^{8}B neutrino spectrum deduced from four laboratory experiments shows a difference with the theoretical prediction at most of 1% [62,65–68]. Accordingly, we will consider that the electron-neutrino energy spectrum of a solar nuclear reaction at the specific location where these neutrinos are created is identical to the equivalent neutrino spectrum measured in the laboratory.

All neutrinos produced in the Sun's nuclear reactions are of an electron-neutrino type. It is only during the propagation phase that these neutrinos vary their flavor among electron, τ and μ. Suitably, we define the original energy spectrum of electron neutrinos by $\Psi_e^s(E)$ and the end energy spectrum of neutrinos after the neutrino flavor oscillations by $\Psi_e^\odot(E)$. The first spectrum, which is identical to the neutrino spectrum obtained in an Earth laboratory, relates to the neutrinos produced in nuclear reactions (see Fig. 1). The latter spectrum corresponds to neutrinos that have their flavor modified by the vacuum oscillations and the generalized MSW oscillation mechanism.

Conveniently, the neutrino spectra $\Psi_e^s(E)$ and $\Psi_e^\odot(E)$ associated to each of the different solar nuclear reactions of the pp chain and CNO cycle are labeled by a unique subscript j which can take one of these values: PP, HeP, ^8B, ^{13}N, ^{15}O or ^{17}F. Hence, the two previous neutrino energy spectra have a simple relation, which reads

$$\Psi_{e,j}^\odot(E) = \langle P_e(E)\rangle_j \Psi_{e,j}^s(E), \tag{24}$$

where $\langle P_e(E)\rangle_j$ is the survival probability of an electron neutrino of energy E. Figure 6 shows the shape of several neutrino spectra $\Psi_{e,j}^\odot(E)$. The final neutrino energy spectrum $\Psi_{e,j}^\odot(E)$ is significantly different from the original

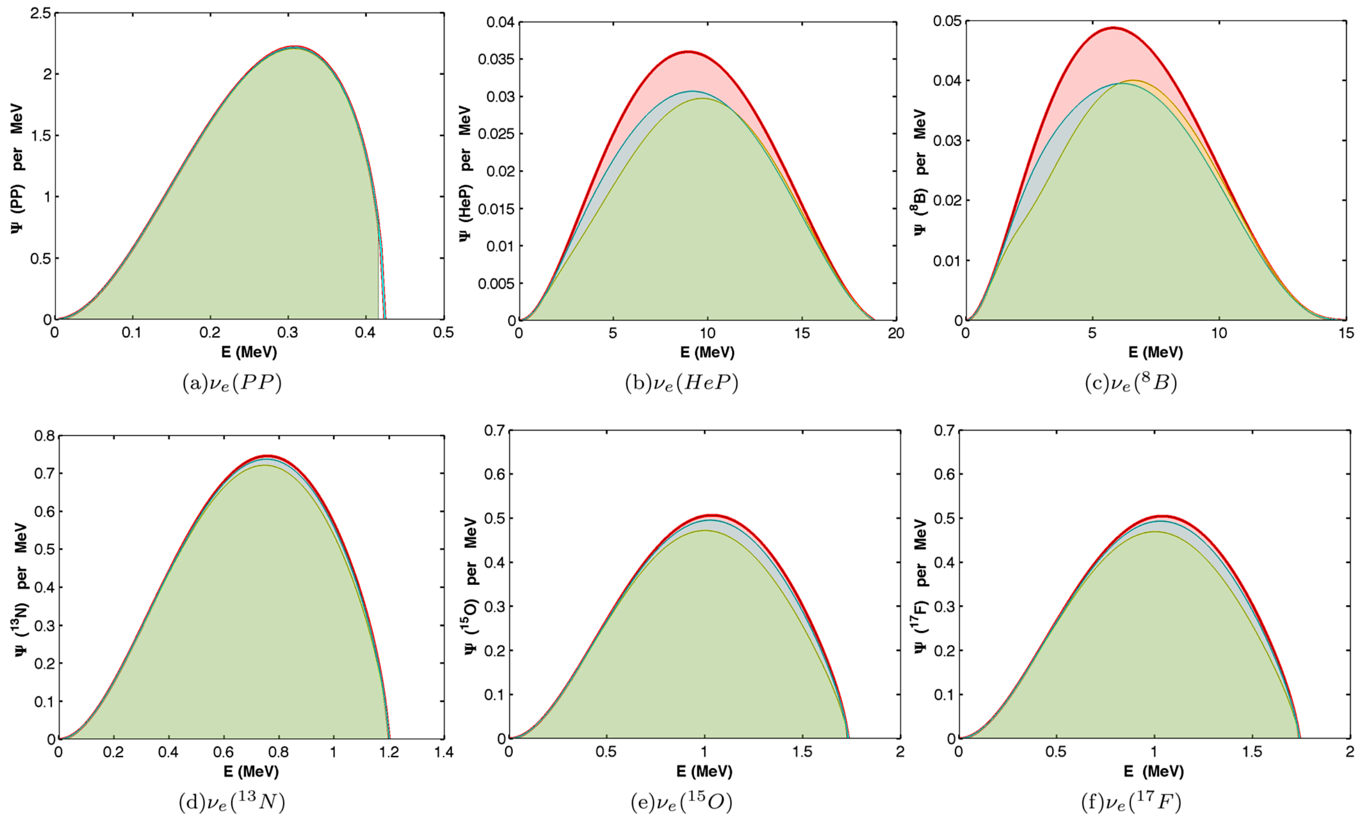

FIG. 6. pp chain and CNO-cycle energy neutrino spectra. $\Psi_{e,j}^\odot(E)$ is the electron solar neutrino spectrum for the standard MSW effect (red area); the other color curves correspond to $\Psi_\odot^{e,j}(E)$, for which the generalized MSW effect is taken into consideration: NSI neutrino interaction with up quarks (blue area), and NSI neutrino interaction with down quarks (green area). $\Psi_{e,j}^\odot(E)$ is defined as the probability per MeV of an electron neutrino with energy E. In the calculation of these neutrino spectra we used an up-to-date standard solar model.

spectrum $\Psi^{s}_{e,j}(E)$. Indeed, while $\Psi^{s}_{e,j}(E)$ depends only on the properties of the nuclear reaction, $\Psi^{\odot}_{e,j}(E)$ becomes distinct from $\Psi^{s}_{e,j}(E)$ due to the contribution of neutrino flavor oscillations. Specifically, $\Psi^{\odot}_{e,j}(E)$ depends on the fundamental parameters related with the neutrino vacuum oscillations through the (generalized) MSW oscillation mechanism, which depends on the local densities of electrons and quarks, and the NSI coupling constants [69]. As discussed previously, all these effects are taken into account in $\langle P_e(E)\rangle_j$ [Eq. (23)]. In this study, we do not include the monoenergetic spectral lines of pp chain nuclear reactions PeP and ^7Be. Although the previous result [Eq. (24)] also holds for these two neutrino sources (corresponding to the sources marked with the subscript $_*$ in Fig. 1), we opt not to include them in this study, since for these neutrino sources other solar plasma properties contribute to change the shape of the neutrino spectral lines.

Figure 6 shows the spectra of electron neutrinos for some of the leading nuclear reactions of the Sun's core. The general shape of the spectra $\Psi^{\odot}_{e,j}(E)$ [Eq. (24)] is a combination of the neutrino spectrum of the nuclear reaction $\Psi^{\odot}_{e,j}(E)$ and $\langle P_e(E)\rangle_j$ which depends on the local density of electrons, down quarks and up quarks, as well as of the NSI parameters of the generalized MSW mechanism. For the specific set of NSI parameters discussed in this study, clearly the HeP and ^8B neutrino emission show the larger variation of the shape of their spectra.

In both cases the interaction of neutrinos with (up and down) quarks leads to neutrino spectra with quite distinct shapes (the blue and green areas in Fig. 6) from the ones found in the standard MSW neutrino interaction (red area in Fig. 6). Equally important is the fact that it is possible to distinguish between the two neutrino models of interaction with quarks, since each model depends differently on the neutrino energy. The ^{15}O and ^{17}F nuclear reactions also show neutrino spectra with different shapes, although in this case the impact of the NSI interactions is much less pronounced than in the previous case, at least for the current set of parameters. For the two other nuclear reactions, PP and ^{13}N, the impact of the NSI interactions is very small. This is somehow expected since the energy of the neutrinos emitted in these nuclear reactions is relatively small. For this neutrino energy range the flavor oscillations are dominated by vacuum oscillations and are almost independent of matter oscillations.

V. CONCLUSION

In this study we have computed the expected alteration in the shape of some leading solar neutrino spectra resulting from neutrinos having a new type of interaction with up and down quarks, identical to the MSW oscillations of neutrinos with electrons. This new type of matter interaction, also known as generalized MSW oscillations, depends on the specific properties of the neutrino interaction model but also on the local thermodynamic properties of the Sun's interior.

The study shows that the neutrino spectra of the different solar nuclear reactions have quite distinct sensitivities to the new neutrino physics. The HeP and ^8B neutrino spectra have their shapes more affected by the new interaction between neutrinos and quarks. The ^{15}O and ^{17}F neutrino spectra also have a small alteration to their shapes, but these effects are much less pronounced than in the previous case. The impact of new physics in the PP and ^{13}N spectra is also very small.

The new generation of neutrino experiments, such as the Low Energy Neutrino Astronomy (LENA) [6], the Jiangmen Underground Neutrino Observatory (JUNO) [7], Jinping Neutrino Experiment [10], the Deep Underground Neutrino Experiment (DUNE) [8], and the NOνA Neutrino Experiment [9], will allow researchers to test some of the new neutrino physics theories. The most promising evidence to discover NSI in solar neutrino data is the precise measurement of the ^8B spectrum. Conveniently, we have estimated how the experimental error of the next generation of detectors like LENA [70] could affect our conclusions. Figure 7 shows an error bar estimation of the ^8B spectrum computed assuming the error in the survival probability is $P_e(E) \pm 0.025$, which is the possible precision that could be obtained for the electron-neutrino survival probability after 5 years of LENA measurements [70]. Even in a relatively short period of 5 years of neutrino observations, it is already possible to find if neutrinos are

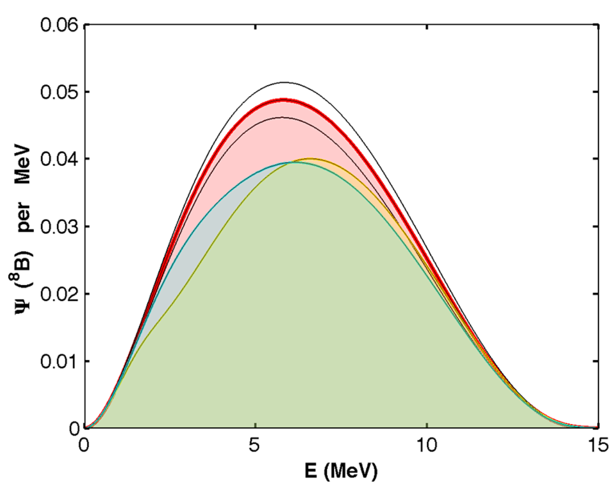

FIG. 7. $\Psi^{\odot}_{e,^8B}(E)$ is the electron solar neutrino spectrum for the standard MSW effect (red area) with the error bar computed for the forthcoming LENA experiment. The error (black lines) in the spectrum shape is computed assuming the error in the survival probability is $P_e(E) \pm 0.025$, which corresponds to 5 years of LENA measurements. The colored curves follow the same color scheme shown in Fig. 6. For clarity we have not included the error bar in the two other curves. Nevertheless, we note that the error bars for the other curves are identical to this one.

experiencing flavor oscillations due to their interaction with quarks. Indeed, the identification by a future solar neutrino detector of a strong distortion in the shape of the solar neutrino spectrum, like the ^8B neutrino spectrum compared to the one predicted by the standard solar model, will constitute a strong indication for the existence of interactions between neutrinos and quarks in the Sun's core. The location and magnitude of the distortion of the solar spectrum should give us some indication about the type of interaction (i.e., up quarks, down quarks or both).

In conclusion, we have shown that in the near future neutrino spectroscopic measurements will be used to infer the new interaction between neutrinos and quarks. This will be an important and totally independent way of testing new neutrino physics interaction models.

ACKNOWLEDGMENTS

This work was supported by Grants from Fundação para a Ciência e Tecnologia and Fundação Calouste Gulbenkian. The author thanks the anonymous referee for the comments and suggestions made to this work.

APPENDIX: DIMENSIONLESS PARAMETERS ENCODING THE DEVIATION FROM STANDARD INTERACTIONS

The interactions of neutrinos with matter in the theoretical framework of the nonstandard model (e.g., [57]) can be described by the Lagrangian term given by Eq. (19). In the following, it is assumed that electron neutrinos couple only with the up quarks and down quarks of the solar plasma (see Sec. III E for details). For convenience, we adopt the parametrization of Gonzalez-Garcia and Maltoni [57], Maltoni and Smirnov [59], and Friedland *et al.* [60] in which the coupling of electron neutrinos with either up quarks or down quarks of the solar plasma is parametrized by a set of two independent parameters $(\epsilon_N^u, \epsilon_D^u)$ or $(\epsilon_N^d, \epsilon_D^d)$. Accordingly, the coefficients ϵ_D^f and ϵ_N^f relate to the original parameters $\epsilon_{\alpha\beta}$ as

$$\begin{aligned}\epsilon_D^f = {} & c_{12}s_{13}Re[e^{i\delta_{CP}}(s_{23}\epsilon_{e\mu}^f + c_{23}\epsilon_{e\tau}^f)] \\ & -(1+s_{13}^2)c_{23}s_{23}Re(\epsilon_{\mu\tau}^f) - \frac{c_{13}^2}{2}(\epsilon_{ee}^f - \epsilon_{\mu\mu}^f) \\ & + \frac{s_{23}^2 - s_{13}^2c_{23}^2}{2}(\epsilon_{\tau\tau}^f - \epsilon_{\mu\mu}^f) \end{aligned} \tag{A1}$$

and

$$\begin{aligned}\epsilon_N^f = {} & c_{13}(c_{23}\epsilon_{e\mu}^f - s_{23}\epsilon_{e\tau}^f) \\ & + s_{13}e^{-i\delta_{CP}}[s_{23}^2\epsilon_{\mu\tau}^f - c_{23}^2\epsilon_{\mu\tau}^{f*} + c_{23}s_{23}(\epsilon_{\tau\tau}^f - \epsilon_{\mu\mu}^f)]. \end{aligned} \tag{A2}$$

As in this work we are only interested in the interaction of neutrinos with the solar plasma, we will consider at a time the following values of f: e, u and d. A detailed discussion about the relevance of this parametrization can be found in Gonzalez-Garcia and Maltoni (e.g., [57]) and Friedland *et al.* (e.g., [60]).

[1] C. K. Jung, T. Kajita, T. Mann, and C. McGrew, Oscillations of atmospheric neutrinos, Annu. Rev. Nucl. Part. Sci. **51**, 451 (2001).

[2] T. Kajita and Y. Totsuka, Observation of atmospheric neutrinos, Rev. Mod. Phys. **73**, 85 (2001).

[3] Q. R. Ahmad *et al.*, Measurement of the Rate of $\nu_e + d \to p + p + e^-$ Interactions Produced by ^{8}B Solar Neutrinos at the Sudbury Neutrino Observatory, Phys. Rev. Lett. **87**, 071301 (2001).

[4] R. Davis, D. S. Harmer, and K. C. Hoffman, Search for Neutrinos from the Sun, Phys. Rev. Lett. **20**, 1205 (1968).

[5] W. C. Haxton, R. G. H. Robertson, and A. M. Serenelli, Solar neutrinos: Status and prospects, Annu. Rev. Astron. Astrophys. **51**, 21 (2013).

[6] M. Wurm *et al.*, The next-generation liquid-scintillator neutrino observatory LENA, Astropart. Phys. **35**, 685 (2012).

[7] F. An *et al.*, Neutrino physics with JUNO, J. Phys. G **43**, 030401 (2016).

[8] A. de Gouvêa and K. J. Kelly, Non-standard neutrino interactions at DUNE, Nucl. Phys. **908B**, 318 (2016).

[9] A. Friedland and I. M. Shoemaker, Searching for novel neutrino interactions at NOvA and beyond in light of large theta_13, arXiv:1207.6642.

[10] J. F. Beacom *et al.*, Letter of intent: Jinping Neutrino Experiment, arXiv:1602.01733.

[11] A. Bandyopadhyay *et al.*, Physics at a future neutrino factory and super-beam facility, Rep. Prog. Phys. **72**, 106201 (2009).

[12] A. de Gouvea *et al.*, Neutrinos, arXiv:1310.4340.

[13] A. B. Balantekin and H. Yüksel, Physics potential of solar neutrino experiments, Nucl. Phys. B, Proc. Suppl. **138**, 347 (2005).

[14] A. B. Balantekin, J. F. Beacom, and J. M. Fetter, Matter-enhanced neutrino oscillations in the quasi-adiabatic limit, Phys. Lett. B **427**, 317 (1998).

[15] I. Lopes, Search for global f-modes and p-modes in the ^{8}B neutrino flux, Astrophys. J. Lett. **777**, L7 (2013).

[16] A. Serenelli, C. Peña-Garay, and W. C. Haxton, Using the standard solar model to constrain solar composition and nuclear reaction S factors, Phys. Rev. D **87**, 043001 (2013).
[17] I. P. Lopes and J. Silk, Solar neutrinos: Probing the Quasi-Isothermal Solar Core Produced by Supersymmetric Dark Matter Particles, Phys. Rev. Lett. **88**, 151303 (2002).
[18] R. Wendell *et al.*, Atmospheric neutrino oscillation analysis with subleading effects in Super-Kamiokande I, II, and III, Phys. Rev. D **81**, 092004 (2010).
[19] P. Adamson *et al.*, Electron Neutrino and Antineutrino Appearance in the Full MINOS Data Sample, Phys. Rev. Lett. **110**, 171801 (2013).
[20] K. Abe, J. Adam, H. Aihara, T. Akiri, C. Andreopoulos, S. Aoki, A. Ariga, T. Ariga, S. Assylbekov, D. Autiero *et al.*, Observation of Electron Neutrino Appearance in a Muon Neutrino Beam, Phys. Rev. Lett. **112**, 061802 (2014).
[21] O. G. Miranda and H. Nunokawa, Non standard neutrino interactions: Current status and future prospects, New J. Phys. **17**, 095002 (2015).
[22] T. Ohlsson, Status of non-standard neutrino interactions, Rep. Prog. Phys. **76**, 044201 (2013).
[23] I. Girardi, D. Meloni, and S. T. Petcov, The Daya Bay and T2K results on $\sin^2\theta_{13}$ and non-standard neutrino interactions, Nucl. Phys. **B886**, 31 (2014).
[24] S. Turck-Chieze and I. Lopes, Toward a unified classical model of the sun: On the sensitivity of neutrinos and helioseismology to the microscopic physics, Astrophys. J. **408**, 347 (1993).
[25] P. Morel, CESAM: A code for stellar evolution calculations, Astron. Astrophys. Suppl. Ser. **124**, 597 (1997).
[26] M. Asplund, N. Grevesse, and A. J. Sauval, The solar chemical composition, in *Cosmic Abundances as Records of Stellar Evolution and Nucleosynthesis*, Astronomical Society of the Pacific Conference Series Vol. 336, edited by T. G. Barnes, III and F. N. Bash (Astronomical Society of the Pacific, San Francisco, 2005), p. 25.
[27] M. Asplund, N. Grevesse, A. J. Sauval, and P. Scott, The chemical composition of the sun, Annu. Rev. Astron. Astrophys. **47**, 481 (2009).
[28] S. Turck-Chièze and S. Couvidat, Solar neutrinos, helioseismology and the solar internal dynamics, Rep. Prog. Phys. **74**, 086901 (2011).
[29] S. Turck-Chièze, S. Couvidat, L. Piau, J. Ferguson, P. Lambert, J. Ballot, R. A. García, and P. Nghiem, Surprising Sun: A New Step Towards a Complete Picture?, Phys. Rev. Lett. **93**, 211102 (2004).
[30] J. N. Bahcall, S. Basu, M. Pinsonneault, and A. M. Serenelli, Helioseismological implications of recent solar abundance determinations, Astrophys. J. **618**, 1049 (2005).
[31] J. N. Bahcall, A. M. Serenelli, and S. Basu, New solar opacities, abundances, helioseismology, and neutrino fluxes, Astrophys. J. **621**, L85 (2005).
[32] A. M. Serenelli, S. Basu, J. W. Ferguson, and M. Asplund, New solar composition: The problem with solar models revisited, Astrophys. J. Lett. **705**, L123 (2009).
[33] J. A. Guzik and K. Mussack, Exploring mass loss, low-Z accretion, and convective overshoot in solar models to mitigate the solar abundance problem, Astrophys. J. **713**, 1108 (2010).
[34] S. Turck-Chièze, A. Palacios, J. P. Marques, and P. A. P. Nghiem, Seismic and dynamical solar models. I. The impact of the solar rotation history on neutrinos and seismic indicators, Astrophys. J. **715**, 1539 (2010).
[35] S. Turck-Chièze and I. Lopes, Solar-stellar astrophysics and dark matter, Res. Astron. Astrophys. **12**, 1107 (2012).
[36] N. Grevesse and A. J. Sauval, Standard solar composition, Space Sci. Rev. **85**, 161 (1998).
[37] S. Vagnozzi, K. Freese, and T. H. Zurbuchen, A successful solar model using new solar composition data, arXiv: 1603.05960.
[38] M. C. Gonzalez-Garcia and M. Maltoni, Phenomenology with massive neutrinos, Phys. Rep. **460**, 1 (2008).
[39] G. Bellini, L. Ludhova, G. Ranucci, and F. L. Villante, Neutrino oscillations, Adv. High Energy Phys. **2014**, 191960 (2014).
[40] D. K. Papoulias and T. S. Kosmas, Standard and non-standard neutrino-nucleus reactions cross sections and event rates to neutrino detection experiments, Adv. High Energy Phys. **2015**, 763648 (2015).
[41] S. Davidson, C. P. na-Garay, N. Rius, and A. Santamaria, Present and future bounds on non-standard neutrino interactions. J. High Energy Phys. 3 (2003) 011.
[42] T. W. Donnelly and J. D. Walecka, Semi-leptonic weak and electromagnetic interactions with nuclei: Isoelastic processes, Nucl. Phys. **A274**, 368 (1976).
[43] D. Nötzold and G. Raffelt, Neutrino dispersion at finite temperature and density, Nucl. Phys. **B307**, 924 (1988).
[44] K. A. Olive (Particle Data Group Collaboration), Review of particle physics, Chin. Phys. C **38**, 090001 (2014).
[45] C. Giunti and W. K. Chung, *Fundamentals of Neutrino Physics and Astrophysics* (Oxford University Press, New York, 2007).
[46] T. K. Kuo and J. Pantaleone, Neutrino oscillations in matter, Rev. Mod. Phys. **61**, 937 (1989).
[47] K. Huitu, T. J. Kärkkäinen, J. Maalampi, and S. Vihonen, Constraining the nonstandard interaction parameters in long baseline neutrino experiments, Phys. Rev. D **93**, 053016 (2016).
[48] J. Bergström, M. C. Gonzalez-Garcia, M. Maltoni, and T. Schwetz, Bayesian global analysis of neutrino oscillation data, J. High Energy Phys. 9 (2015) 200.
[49] M. C. Gonzalez-Garcia, M. Maltoni, and T. Schwetz, Updated fit to three neutrino mixing: Status of leptonic *CP* violation, J. High Energy Phys. 11 (2014) 52.
[50] M. Apollonio and A. Baldini, Limits on neutrino oscillations from the CHOOZ experiment, Phys. Lett. B **466**, 415 (1999).
[51] G. L. Fogli, E. Lisi, A. Marrone, A. Palazzo, and A. M. Rotunno, Neutrino oscillations, global analysis and theta (13), arXiv:0905.3549.
[52] G. L. Fogli, E. Lisi, A. Marrone, D. Montanino, A. Palazzo, and A. M. Rotunno, Global analysis of neutrino masses, mixings, and phases: Entering the era of leptonic *CP* violation searches, Phys. Rev. D **86**, 013012 (2012).
[53] P. Hernandez, Neutrino physics, arXiv:1010.4131.
[54] A. B. Balantekin and H. Yuksel, Global analysis of solar neutrino and KamLAND data, arXiv:hep-ph/0301072.

[55] S. Goswami and A. Y. Smirnov, Solar neutrinos and 1-3 leptonic mixing, Phys. Rev. D **72**, 053011 (2005).
[56] M. Thomson, Modern Particle Physics (Cambridge University Press, Cambridge, UK, 2013).
[57] M. C. Gonzalez-Garcia and M. Maltoni, Determination of matter potential from global analysis of neutrino oscillation data, J. High Energy Phys. 9 (2013) 152.
[58] Y. Farzan, A model for large non-standard interactions of neutrinos leading to the LMA-dark solution, Phys. Lett. B **748**, 311 (2015).
[59] M. Maltoni and A. Y. Smirnov, Solar neutrinos and neutrino physics, Eur. Phys. J. A **52**, 87 (2016).
[60] A. Friedland, C. Lunardini, and M. Maltoni, Atmospheric neutrinos as probes of neutrino-matter interactions, Phys. Rev. D **70**, 111301 (2004).
[61] C. E. Ortiz, A. García, R. A. Waltz, M. Bhattacharya, and A. K. Komives, Shape of the ^{8}B Alpha and Neutrino Spectra, Phys. Rev. Lett. **85**, 2909 (2000).
[62] W. T. Winter, S. J. Freedman, K. E. Rehm, and J. P. Schiffer, The ^{8}B neutrino spectrum, Phys. Rev. C **73**, 025503 (2006).
[63] J. N. Bahcall and B. R. Holstein, Solar neutrinos from the decay of ^{8}B, Phys. Rev. C **33**, 2121 (1986).
[64] J. Napolitano, S. J. Freedman, and J. Camp, Beta and neutrino spectra in the decay of ^{8}B, Phys. Rev. C **36**, 298 (1987).
[65] W. T. Winter, S. J. Freedman, K. E. Rehm, I. Ahmad, J. P. Greene, A. Heinz, D. Henderson, R. V. Janssens, C. L. Jiang, E. F. Moore, G. Mukherjee, R. C. Pardo, T. Pennington, G. Savard, J. P. Schiffer, D. Seweryniak, G. Zinkann, and M. Paul, Determination of the ^{8}B Neutrino Spectrum, Phys. Rev. Lett. **91**, 252501 (2003).
[66] T. Roger *et al.*, Precise Determination of the Unperturbed ^{8}B Neutrino Spectrum, Phys. Rev. Lett. **108**, 162502 (2012).
[67] M. Bhattacharya, E. G. Adelberger, and H. E. Swanson, Precise study of the final-state continua in ^{8}Li and ^{8}B decays, Phys. Rev. C **73**, 055802 (2006).
[68] O. S. Kirsebom *et al.*, Precise and accurate determination of the ^{8}B decay spectrum, Phys. Rev. C **83**, 065802 (2011).
[69] I. Lopes, Probing the Sun's inner core using solar neutrinos: A new diagnostic method, Phys. Rev. D **88**, 045006 (2013).
[70] R. Möllenberg, F. von Feilitzsch, D. Hellgartner, L. Oberauer, M. Tippmann, J. Winter, M. Wurm, and V. Zimmer, Detecting the upturn of the solar ^{8}B neutrino spectrum with LENA, Phys. Lett. B **737**, 251 (2014).